Journal of Geophysical Research: Solid Earth

Supporting Information for

Catastrophic failure: how and when? Insights from 4D in-situ x-ray micro-tomography

A. Cartwright-Taylor[1], I. G. Main[1], I. B. Butler[1], F. Fusseis[1], M. Flynn[1] and A. King[2]

[1]School of Geosciences, University of Edinburgh, James Hutton Road, Edinburgh EH9 3FE, UK. [2]SOLEIL Synchrotron, L'Orme des Merisiers, Saint Aubin, France.

Contents of this file

Additional Supporting Information (Files uploaded separately)

Introduction

This document and associated separate files contains supporting information in the form of text, figures, tables and movies related to the 4D crack network evolution within two Ailsa Craig microgranite samples, which differed only in their degree of starting heterogeneity. These data were created from analysis of x-ray μCT images collected during experiments conducted at SOLEIL synchrotron in December 2016. The samples were deformed by triaxial compression under a constant confining pressure of 15MPa, during which the deformation was imaged in-situ at various stages during each experiment. The text S1-S5 gives additional detail about the data processing and analysis techniques described in the main text. Figures S1 and S3 show crack volume and inter-crack length distributions respectively from one stage of deformation with the associated Poisson errors and the most likely statistical distribution of the data, while Figure S2 shows the results of the Information Criterion used to distinguish the most likely statistical distribution for the crack volumes at all stages of deformation and Figure S4 shows the evolution with strain of the correlation length and the most likely empirical model for each sample. Figures S5 and S6 are zip files containing high resolution png files of the images shown in Figures 4 and 5 respectively in the main text, labelled according to the conventions shown in Tables 3 and 4 respectively. Table S1 relates to Figures 5 and 6 in the main text, showing the total data from which the percentage scales in those figures were derived. Tables S2 and S3 show the

Information Criterion results for the evolution with strain of porosity and the number of cracks for each sample, and relates to Figure 9b,c in the main text. Table S4 shows the Information Criterion results for the evolution with strain of the correlation length and relates to Figure 13a in the main text. Table S5 shows the Information Criterion results for the evolution with stress of the correlation length and relates to Figure 12. Movies S1-S4 are mp4 files showing time-lapse video of the crack network evolution in each sample viewed from two different angles; along and across the loading axis.

Text S1. Image analysis

S1a. Segmentation

The Hessian eigenvectors give the local principal direction of curvature and each of these has a corresponding magnitude (eigenvalue). The eigenvalues represent the magnitude of the largest local contrast change, and the local contrast change in the other two orthogonal principal directions. For narrow fractures with a low intensity on a brighter background, we are interested in the case where one eigenvalue has a high positive value in conjunction with small values for the other two. The corresponding eigenvector is normal to the planar feature (Voorn et al., 2013).

S1b. 3D microcrack orientations and geometries (object-based)

The best-fitting ellipsoid around each individual segmented crack, C, was calculated from the crack's 3D moments of inertia. First-order moments define the crack's center of mass (centroid): $M_x = [\sum_C x_i]/V(C)$, $M_y = [\sum_C y_{i]}/V(C)$ and $M_z = [\sum_C z_i]/V(C)$, where $V(C)$ is the volume of the crack and (x_i, y_i, z_i) is a point in the crack. Second-order moments define the inertia (or covariance) matrix, I: $I_{xx} = [\sum_C (x_i - M_x)^2]/V(C)$, $I_{yy} = [\sum_C (y_i - M_y)^2]/V(C)$, $I_{zz} = [\sum_C (z_i - M_z)^2]/V(C)$, $I_{xy} = [\sum_C (x_i - M_x)(y_i - M_y)]/V(C)$, $I_{xz} = [\sum_C (x_i - M_x)(z_i - M_z)]/V(C)$ and $I_{yz} = [\sum_C (y_i - M_y)(z_i - M_z)]/V(C)$, with eigenvalues corresponding to ellipsoid radii as described in the main text and eigenvectors representing ellipsoid axes orientations. The eigenvector corresponding to the largest eigenvalue in I is the orientation of the major ellipsoid axis and to the smallest eigenvalue is the orientation of the minor ellipsoid axis, and so on.

Text S2. Akaike Information Criterion calculation

Calculated from the sum of squared errors, SSE, as follows: $AIC = n\, ln(SSE/n) + 2k$, where n is the number of observations in the sample and k is the number of parameters in the model, i.e., the number of parameters in the model equation plus 1 to account for the error (Burnham and Anderson, 2002). This value was then corrected as follows: $AICc = AIC + (2k(k+1))/(n-k-1)$, appropriate in the case that $n < 40k$, which is true here as the number of µCT scans in each experiment is < 40. Then, $\Delta AICc = AICc_{min} - AICc_i$ and the likelihood of model g_i, given the data is $\mathcal{L}(g_i|x) = e^{(\Delta AICc/2)}$, representing the relative likelihood that g_i (with $AICc_i$) is equally as good as g_{min} (with $AICc_{min}$).

Text S3. Maximum likelihood β-value estimation and Bayesian Information Criterion

We first estimated the β-parameter for the characteristic Pareto distribution. The logarithm of the likelihood function, ℓ, for n observations of fracture volume, V_i, is: $\ell = n[\beta \log(V_t) + \log(\beta)] - (1+\beta)\sum_{i=1}^{n} \log V_i$ (eqn. 21 in Kagan, 2002). Optimization of this function was carried out by minimizing the negative log-likelihood ($-\ell$) using the fminsearch MATLAB function. Similar optimizations of the two-parameter log-likelihood functions for the

truncated and tapered Pareto distributions (eqns. 26 and 37 respectively in Kagan, 2002) did not converge so we used the β-parameter estimate from the characteristic Pareto distribution together with the one-parameter estimations presented in Kagan (2002) to determine the unbiased V_c-parameter (corner volume) for (i) the truncated Pareto: $V_c = V_{max}\{1 + 1/n\beta[(V_{max}/V_t)^{\beta} - 1]\}$ (Pisarenko, 1991; Kijko and Graham, 1998; eqn. 27 in Kagan 2002), and (ii) the tapered Pareto based on statistical moments of the volume distribution: $V_{cm} = [\sum V_i^2/n - V_t^2]/2[V_t\beta + (1-\beta)\bar{V}]$, where $\bar{V} = \frac{1}{n}\sum V_i$ is the average fracture volume (Kagan and Schoenberg, 2001; eqn. 35 in Kagan, 2002).

We then used a modified Bayesian Information Criterion (BIC) to distinguish between the three competing models (Bell et al., 2013a), introducing an appropriate penalty for the additional parameters V_c and V_{cm} in the TRP and TAP models respectively: $BIC = -2\ln(\ell) + k\ln(n)$, where ℓ is the likelihood function, n is the total number of events and k is the number of model parameters, including the error (Leonard and Hsu, 1999). The difference is then: $\Delta BIC_{GR-TRP} = -2(\Delta\ln(\ell)) + \ln(n)$. In this notation, the preferred model has the lower BIC so in the case described (GR-TRP), $\Delta BIC < 0$ if the unrestricted Pareto model (GR) is preferred and $\Delta BIC > 0$ if the truncated Pareto model (TRP) is preferred. The same calculation was performed to compare the unrestricted Pareto model (GR) with the tapered Pareto model (TAP): ΔBIC_{GR-TAP}.

Text S4. Estimation of two-point correlation dimension D

If the number of features N with a characteristic linear dimension greater than r (complementary cumulative) satisfies the condition $N(r \geq r_i) \sim r^{-D}$, then a fractal is defined with a fractal dimension D (Turcotte, 1997). The derivative of this condition is then $dN \sim r^{-D-1}\,dr$. This translates in our case, for finite inter-crack lengths L_i with a higher probability of large inter-crack lengths than small ones, to a cumulative probability density function, $P(L \leq L_i) \propto {L_i}^D$ and an incremental probability density function, $P_i \propto {L_i}^{D-1}$. The exponent, $D_{inc} = D - 1$, of the PDF of L_i in the identified power-law region, $30 < L_i < 1350$ µm, was obtained from the gradient of the best-fitting linear regression model in log-log space (Figure S3). From this the fractal dimension, $D = D_{inc} + 1$. Confirmation of D was obtained from a separate but equivalent modelling of the cumulative distributions, $P(L \leq L_i)$ for $30 < L_i < 1350$ µm, which showed that $D_{cum} \sim D_{inc} + 1$.

Text S5. Inverse power-law parameters for correlation length, ξ as a function of stress, σ

The model $\xi/l = k(\sigma_p - \sigma)^{-p}$, where ξ is the correlation length, l is the length of the analyzed sub-volume and σ is the differential stress has parameters k, σ_p (predicted failure stress) and p. We used the MATLAB function lsqcurvefit with the trust-region-reflective algorithm to obtain the parameters by non-linear regression, i.e., by minimizing the sum of residuals between the model function and the observed data. Initial values for k and p were obtained from a linear regression in loglog space of the observed data, ξ against $(\sigma_f - \sigma)$ where σ_f is the observed failure stress, $\log k$ is the zero cut-off and p is the absolute value of the gradient. The initial value of σ_p was 200; close to the observed values of 185 and 182. Bounds were chosen as follows: $0 < k < 1000$, $0 < \sigma_p < 1000$ and $0.1 < p < 6$.

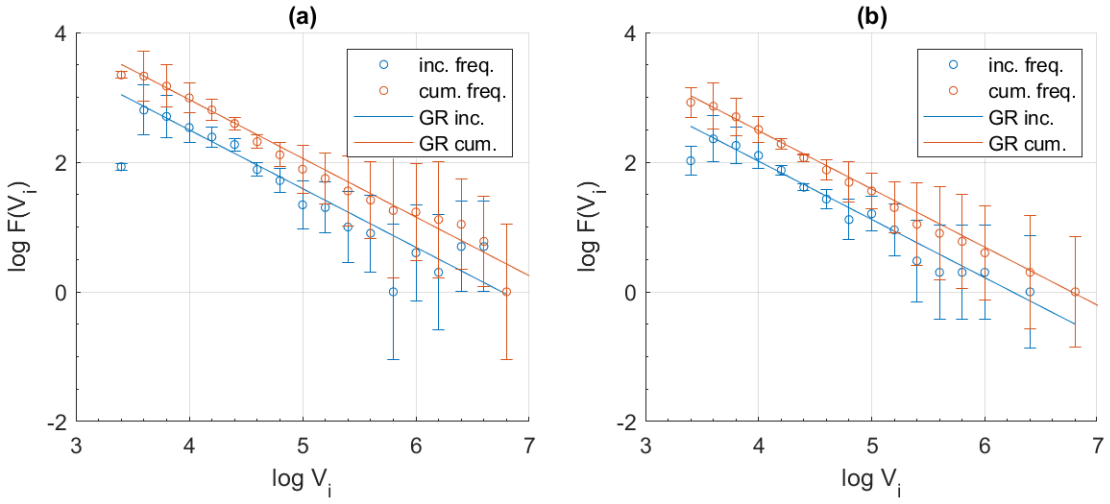

Figure S1. Examples of the incremental frequency-volume distribution (blue circles) and the cumulative complementary distribution (orange circles) at (**a**) 97% of peak stress in the untreated sample and (**b**) peak stress in the heat-treated sample. Blue and orange lines show the preferred GR model (incremental and cumulative respectively). Error bars show the Poisson counting errors (Greenhough and Main, 2008). The completeness volume V_t is shown at the peak of the incremental distribution ($\log V_t$), i.e., the highest value of the first derivative of the cumulative frequency-volume function, which corresponds to the largest microcrack volume with the maximum incremental probability.

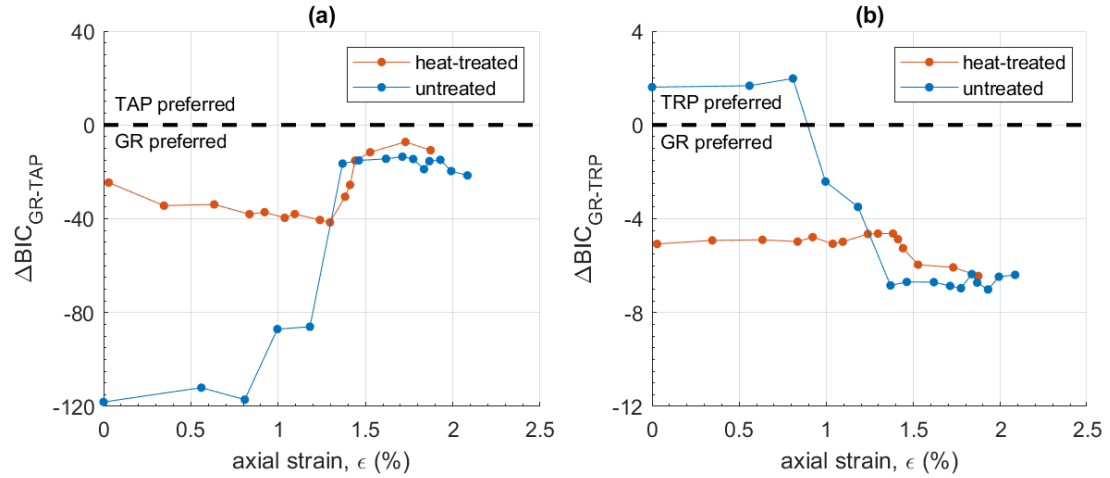

Figure S2. (**a**) ΔBIC_{GR-TRP} and (**b**) ΔBIC_{GR-TAP} evolution with strain for the untreated (blue) and heat-treated (orange) samples showing that both samples preferred the GR model over the TAP. The untreated sample preferred the TRP model early on and then transitioned to the GR model, while the heat-treated sample preferred the GR model for the whole experiment.

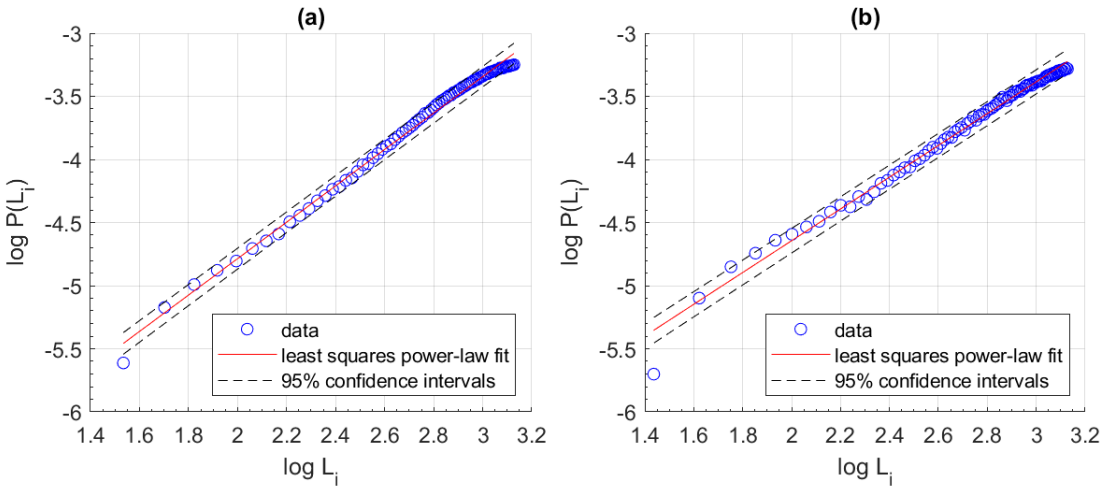

Figure S3. Examples of inter-void length incremental frequency distributions in log-log space with best-fitting linear model and 95% confidence intervals at (**a**) 97% of peak stress in the untreated sample and (**b**) peak stress in the heat-treated sample.

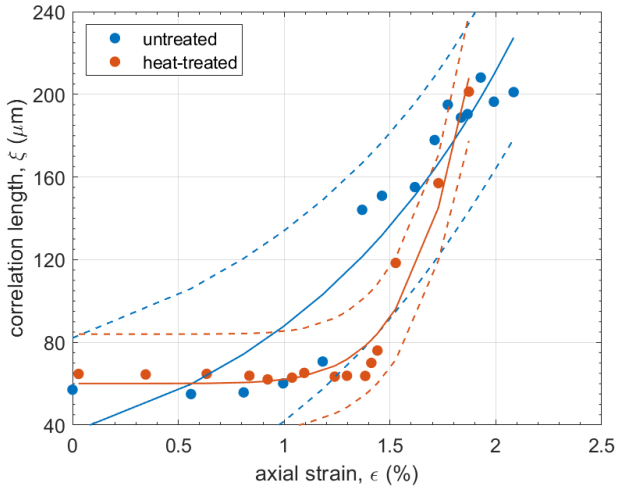

Figure S4. Evolution of correlation length with strain for both samples, with their most likely relationship. In untreated sample this relationship is exponential: $\xi = 36.6\exp^{0.877\pm0.226\epsilon}$, and for in the heat-treated sample it is a power-law: $\xi = 1.95\epsilon^{6.90\pm2.12} + 60.1$. See also Table S4.

Figure S5. Zip file containing high resolution images of crack evolution in the untreated sample (Figure 5 in main text – y, z projection). Filename: fs04_high-res_untreated_sample

Figure S6. Zip file containing high resolution images of crack evolution in the heat-treated sample (Figure 6 in main text – y, z projection). Filename: fs05_high-res_heat-treated_sample

µCT scan	Untreated sample [ACfresh02]	Heat-treated sample [ACHT01]
A	0.143±0.118	0.330±0.151
B	0.179±0.125	0.324±0.157
C	0.147±0.127	0.496±0.142
D	0.185±0.120	0.516±0.167
E	0.169±0.129	0.495±0.152
F	0.167±0.115	0.556±0.142
G	0.171±0.102	0.496±0.134
H	0.212±0.103	0.590±0.162
I	0.176±0.107	0.713±0.164
J	0.147±0.103	0.611±0.165
K	0.141±0.139	0.597±0.147
L	0.132±0.145	0.714±0.179
M	0.139±0.114	0.735±0.129
N	0.111±0.132	0.760±0.133
O	0.142±0.144	0.962±0.140
P	0.592±0.171	0.683±0.109

Table S1. Degree of anisotropy in void strike, θ, with 95% confidence intervals determined from regression of model $P_\theta = \overline{P_\theta} + A\sin(2\theta)$. Each distribution contains 46 bins ($n = 46$).

model [for ACfresh02]	$AICc$ for φ	$AICc$ for N
quadratic: $\boldsymbol{y = ax^2 + bx + c}$	-98.10	154.84
exponential 1: $\boldsymbol{y = ae^{bx}}$	-96.24	162.38
exponential 2: $\boldsymbol{y = ae^{bx} + ce^{dx}}$	-88.70	158.82
power 1: $\boldsymbol{y = ax^b}$	**-100.05**	180.04
power 2: $\boldsymbol{y = ax^b + c}$	-97.94	**154.55**
summary	38% chance that quad, 35% that pow2 and <15% other models are good as pow1.	86% likelihood that quad and <12% that other models are good as pow2.

Table S2. Corrected Akaike Information Criterion ($AICc$) for porosity, φ, and the number of microcracks, N, with strain, ϵ, regression model fits for the untreated sample [ACfresh02]. Lowest values are highlighted bold showing that power-law accelerations are preferred; of the form $y = ax^b$ for φ and $y = ax^b + c$ for N. The most likely models for the untreated sample are $\varphi_{UT} = 0.05\epsilon^{3.14\pm0.570}$ and $N_{UT} = 175\epsilon^{3.08\pm1.10} + 926$.

model [for ACHT01]	$AICc$ for φ	$AICc$ for N
quadratic: $y = ax^2 + bx + c$	-109.53	124.46
exponential 1: $y = ae^{bx}$	-119.38	137.83
exponential 2: $y = ae^{bx} + ce^{dx}$	-148.22	98.09
power 1: $y = ax^b$	-115.19	145.27
power 2: $y = ax^b + c$	**-152.19**	**94.37**
summary	14% chance that exp2 and <0.01% that remaining models are as good as pow2.	16% chance that exp2 and <0.01% that remaining models are as good as pow2.

Table S3. Corrected Akaike Information Criterion ($AICc$) for porosity, φ, and the number of microcracks, N, with strain, ϵ, regression model fits for the heat-treated sample [ACHT01]. Lowest values are highlighted bold showing that a power-law acceleration of the form $y = ax^b + c$ is the preferred model for both variables. The most likely models for the heat-treated sample are $\varphi_{HT} = 0.0006\epsilon^{8.80\pm1.38} + 0.025$ and $N_{HT} = 3.17\epsilon^{7.66\pm1.60} + 516$.

model	$AICc$	
	ACfresh02	ACHT01
linear: $y = ax + b$	103.05	111.59
quadratic: $y = ax^2 + bx + c$	96.34	96.77
exponential 1: $y = ae^{bx}$	**95.78**	103.72
exponential 2: $y = ae^{bx} + ce^{dx}$	104.02	82.713
power 1: $y = ax^b$	99.54	111.61
power 2: $y = ax^b + c$	96.50	**78.27**
summary	75% chance that quad, 70% that pow2 and <15% that remaining models are good as exp1.	<11% chance that other models are as good as pow2.

Table S4. Corrected Akaike Information Criterion ($AICc$) for correlation length, ξ, with strain, ϵ, from regression model fits for both the untreated sample [ACfresh02] and the heat-treated sample [ACHT01]. Lowest values showing the preferred model are highlighted in bold. The most likely model for the untreated sample is an exponential: $\xi = 36.6\exp^{0.877\pm0.226\epsilon}$, and for the heat-treated sample is a power-law: $\xi = 1.95\epsilon^{6.90\pm2.12} + 60.1$.

model	$AICc$	
	ACfresh02	**ACHT01**
exponential: $y = ae^{bx}$	**-113.46**	-66.20
inverse power-law: $y = k(x_p - x)^{-p}$	-106.53	**-66.86**
$\Delta AICc = AICc_{min} - AICc_i$	-6.93	-0.66
$\mathcal{L}(g_i\|x) = e^{(\Delta AICc/2)}$	0.03	0.72
summary	3% chance that inverse power-law fits data as well as exponential	72% chance that exponential fits data as well as inverse power-law

Table S5. Corrected Akaike Information Criterion ($AICc$ – see Text S2 for full details of the calculations) for normalized correlation length, ξ/l, with stress, σ, from non-linear regression model fits for both the untreated sample [ACfresh02] and the heat-treated sample [ACHT01]. Lowest values showing the preferred model are highlighted in bold. The untreated sample prefers the exponential, while the heat-treated sample prefers the inverse power-law. Parameters for these preferred models are provided in Figure 12 in the main text.

Movie S1. Time-lapse video showing crack network evolution in the untreated sample in the (x, y) plane. Filename: ms01_untreated_x-y-plane

Movie S2. Time-lapse video showing crack network evolution in the untreated sample in the (y, z) plane. Filename: ms02_untreated_y-z-plane

Movie S3. Time-lapse video showing crack network evolution in the heat-treated sample in the (x, y) plane. Filename: ms03_heat-treated_x-y-plane

Movie S4. Time-lapse video showing crack network evolution in the heat-treated sample in the (y, z) plane. Filename: ms04_heat-treated_y-z-plane